Icosahedral gold cage clusters: $M@Au_{12}^-$ (M=V, Nb, and Ta)

Hua-Jin Zhai
Department of Physics, Washington State University, Richland, Washington 99352 and W. R. Wiley Environmental Molecular Sciences Laboratory, Pacific Northwest National Laboratory, Richland, Washington 99352

Jun Li
W. R. Wiley Environmental Molecular Sciences Laboratory, Pacific Northwest National Laboratory, Richland, Washington 99352

Lai-Sheng Wang[a)]
Department of Physics, Washington State University, Richland, Washington 99352 and W. R. Wiley Environmental Molecular Sciences Laboratory, Pacific Northwest National Laboratory, Richland, Washington 99352

(Received 26 July 2004; accepted 5 August 2004)

We report the observation and characterization of a series of stable bimetallic 18-valence-electron clusters containing a highly symmetric 12-atom icosahedral Au cage with an encapsulated central heteroatom of Group VB transition metals, $M@Au_{12}^-(M=V,Nb,Ta)$. Electronic and structural properties of these clusters were probed by anion photoelectron spectroscopy and theoretical calculations. Characteristics of the $M@Au_{12}^-$ species include their remarkably high binding energies and relatively simple spectral features, which reflect their high symmetry and stability. The adiabatic electronic binding energies of $M@Au_{12}^-$ were measured to be 3.70 ± 0.03, 3.77 ± 0.03, and 3.76 ± 0.03 eV for $M=V$, Nb, and Ta, respectively. Comparison of density-functional calculations with experimental data established the highly symmetric icosahedral structures for the 18-electron cluster anions, which may be promising building blocks for cluster-assembled nanomaterials in the form of stoichiometric $[M@Au_{12}^-]X^+$ salts. © *2004 American Institute of Physics.*
[DOI: 10.1063/1.1799574]

I. INTRODUCTION

Gold clusters and nanoparticles have become an active research field lately because of the discovery of remarkable catalytic properties of nanogold[1] and their potential applications in nanoelectronics, nanosensors, and as biological markers.[2] The chemistry of gold is dominated by the strong relativistic effects[3] and the so-called aurophilic attraction,[4] leading to highly unusual structures for gold clusters and compounds relative to those for copper and silver. One of the most interesting findings has been the planar gold cluster anions with more than ten atoms.[5–9] These unique planar cluster anions were experimentally discovered using ion mobility,[6] interpreted on the basis of the strong relativistic effects of Au,[5,7] and were further confirmed by a joint photoelectron spectroscopy (PES) and density-functional theory (DFT) study.[8] Among other exciting discoveries in elemental gold clusters include the tetrahedral Au_{20} cluster[10,11] and the golden fullerene Au_{32} cage cluster reported recently.[12,13]

Despite the fact that the bare 13-atom gold cluster anion has been shown not to possess a high symmetry icosahedral (I_h) structure,[6] Pyykkö and Runeberg[14] recently predicted a series of highly stable gold clusters containing an icosahedral Au_{12} cage and a central heteroatom, $M@Au_{12}(M=Ta^-,W,Re^+)$, which is valent isoelectronic to the known I_h Au_{13}^{5+} cage.[15,16] These remarkable clusters were shown to attain their stabilities from the strong relativistic effect, the aurophilic attraction, and the perfect 18-electron bonding to the central heteroatom's $6s$, $6p$, and $5d$ shells.[14,17] Shortly after, we were able to produce experimentally one of these clusters, namely, $W@Au_{12}$, as well as its $4d$ analog $Mo@Au_{12}$, in the form of anions in the gas phase, and characterized their structural and electronic properties using PES and further DFT calculations.[18] Nearly identical PES spectra were observed for $W@Au_{12}^-$ and $Mo@Au_{12}^-$; the closed-shell electronic structure of $W@Au_{12}$ and $Mo@Au_{12}$ were revealed by the observation of a large energy gap in the PES spectra. However, the other two members of the predicted $M@Au_{12}$ clusters have not been experimentally observed and confirmed. The charged nature of $Ta@Au_{12}^-$ and $Re@Au_{12}^+$ suggests that they should be able to be prepared straightforwardly in the gas phase and detected by mass spectrometry. However, the positively charged $Re@Au_{12}^+$ means that it cannot be studied by ultraviolet PES, whereas a very high electron binding energy is expected for $Ta@Au_{12}^-$, making it more challenging to be characterized experimentally.

Following our previous work on $W@Au_{12}^-$ and $Mo@Au_{12}^-$,[18] here we report the successful preparation and confirmation of $Ta@Au_{12}^-$ using PES and DFT calculations. In addition, we also prepared its $4d$ and $3d$ analogs, $Nb@Au_{12}^-$ and $V@Au_{12}^-$, and obtained nearly identical PES spectra for all the three $M@Au_{12}^-(M=Ta,Nb,V)$ clusters. As expected, extremely high electron binding energies were ob-

a)Electronic mail: ls.wang@pnl.gov

served for these three species. Analogous to $W@Au_{12}$ and $Mo@Au_{12}$, our DFT calculations again revealed low-lying O_h and D_{5h} structures. The molecular orbital energy levels and the simulated PES spectra for the I_h clusters are in good agreement with the observed PES spectra, confirming their high symmetry structures and stability. Our results also demonstrate that the Au_{12} cage is highly flexible to accommodate the central heteroatom.

II. EXPERIMENTAL AND COMPUTATIONAL DETAILS

A. Experimental method

The experiment was carried out using a magnetic-bottle time-of-flight PES apparatus equipped with a laser vaporization supersonic cluster source.[19,20] Briefly, the MAu_{12}^- (M = V,Nb,Ta) cluster anions were produced by laser vaporization of the corresponding Au/M mixed target (approximately 10:1 Au/M atom ratio) in the presence of a helium carrier gas. Various mixed cluster anions MAu_n^- were produced from the cluster source and were analyzed using a time-of-flight mass spectrometer. The cluster species of current interest, MAu_{12}^-, was mass selected and decelerated before being photodetached. Two detachment photon energies were used in the current experiments: 266 nm (4.661 eV) and 193 nm (6.424 eV). Photoelectrons were collected at nearly 100% efficiency by the magnetic bottle and analyzed in a 3.5 m long electron flight tube. Photoelectron spectra were calibrated using the known spectrum of Rh^-, and the electron kinetic energy resolution of the apparatus ($\Delta Ek/Ek$) was $\approx$2.5%, i.e., $\sim$25 meV for 1 eV electrons.

B. Computational methods

The calculations were performed using density-functional methods implemented in the Amsterdam Density Functional (ADF) program[21–23] and the NWCHEM program.[24] In the ADF calculations, we used the gradient-corrected exchange-correlation functional of Perdew–Wang 1991 (PW91).[25,26] All the valence and core electrons of the atoms in MAu_{12}^- were included in the variation treatment and uncontracted all-electron Slater basis sets were used with quality of triple-zeta with two polarization functions (TZ2P).[27] The zero-order regular approximation (ZORA) was adopted to account for the scalar and spin-orbit relativistic effects,[28] which are known to be extremely important for 5d systems, particularly for gold.[3] Geometry optimizations were performed for the icosahedral (I_h), octahedral (O_h), and D_{5h} structures to determine the lowest energy geometries of the anions. The total energy calculations including spin-orbit coupling effects were performed at the optimized scalar-relativistic geometries. The second-order energy derivatives were calculated to determine the stationary nature of the different structures.

In the NWCHEM calculations, we used the hybrid B3LYP method, which makes use of the Hartree–Fock exact exchange and Becke's exchange functional and Lee–Yang–Parr correlation functional.[29–32] The Stuttgart energy-consistent quasirelativistic small-core pseudopotentials were used to account for the scalar relativistic effects and to reduce the computational cost for these heavy elements.[33,34] Specifically, the 13 valence electrons for V, Nb, and Ta and the 19 valence electrons for Au were explicitly treated in the variation calculations. The corresponding pseudopotential valence Gaussian basis sets, $(8s7p6d)/[6s5p3d]$ for V, Nb, Ta, and $(8s6p5d)/[7s3p4d]$ for Au, were augmented by adding $2f$ and $1g$ type polarization functions as proposed by Martin and Sundermann.[35] The vertical electron detachment energies (VDEs) were calculated using a combined ΔSCF-TDDFT approach that we outlined before.[10,18] From this approach, the ground-state energies of the anions and the neutral species were calculated via SCF energy difference from the DFT (B3LYP) calculations, whereas the excited states of the electron-detached neutral species were calculated by using TDDFT methods. Since the local density exchange-correlation potentials and most of the gradient-corrected potentials suffer from the notorious wrong asymptotic behavior, TDDFT methods for high-lying excited states and anionic species are known to be unreliable because of the underestimated TDDFT ionization threshold.[36,37] For example, TDDFT tends to underestimate excitation energies for high-lying excited states by up to 1 eV or more.[38,39] We therefore chose to use the B3LYP(AC) self-contained asymptotic correction scheme proposed by Hirata *et al.* to amend the asymptotic problem for applying TDDFT methods to high-lying excited states.[38] In this scheme, use is made of the Casida-Salahub asymptotic correction and the Zhan–Nichols–Dixon linear correlation relation between the experimental ionization energies and the highest occupied Kohn–Sham orbital energies.[40,41] For all the calculations, the extra fine integration grid was used to obtain highly accurate DFT results.

III. EXPERIMENTAL RESULTS

Figure 1 displays the PES spectra of MAu_{12}^- (M = V,Nb,Ta) at 266 and 193 nm. The 266 nm spectrum of VAu_{12}^- [Fig. 1(a)] revealed one intense band (labeled X) with a VDE of 3.79 eV. A similar intense peak was also observed in the 266 nm spectra of $NbAu_{12}^-$ [Fig. 1(b)] and $TaAu_{12}^-$ [Fig. 1(c)] at slightly higher VDEs (Table I).

However, in addition to the similar and intense feature (X) observed in all three spectra at 266 nm, other relatively weak features were also present in these spectra. In the case of VAu_{12}^- [Fig. 1(a)], these features appeared to be continuous starting at $\sim$2.6 eV. In the cases of $NbAu_{12}^-$ and $TaAu_{12}^-$, these features were discrete, but they were different for the two species. These weak features were not associated with the main intense X band in each case, because their relative intensities could be varied, depending on the source conditions, though they could not be eliminated. There were two origins for these weak features: (1) contaminations, and (2) structural isomers. Because of the heavy masses of the MAu_{12}^- species (>2400 amu), the limited mass resolution of our time-of-flight mass spectrometer ($M/\Delta M \sim 400$) did not allow resolution of mass peaks separated by mass/charge ratios of $<\sim$6. Minor contaminations due to oxide, $M_xAu_yO_z^-$, or different M/Au compositions, $M_xAu_y^-$, might contribute to the MAu_{12}^- spectra. Structural isomers

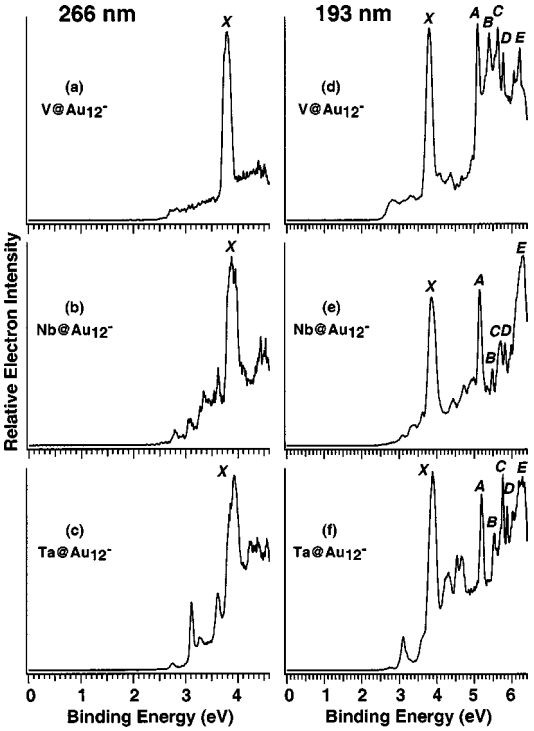

FIG. 1. Photoelectron spectra of $M\mathrm{Au}_{12}^-$ (M=V,Nb,Ta) at 266 nm (4.661 eV) and 193 nm (6.424 eV).

were also possible contributors to the weak features, as will be shown later from the theoretical results. Similar problems existed in our previous work on $\mathrm{W@Au}_{12}^-$ and $\mathrm{Mo@Au}_{12}^-$.[18] However, because of the large HOMO-LUMO (HOMO and LUMO are the highest occupied and lowest unoccupied molecular orbital, respectively) gaps existed in those clusters and the resulting lower electron binding energies, we were able to obtain uncontaminated spectra using a lower detachment energy (2.331 eV).[18] Nevertheless, we were confident that the intense X band in the 266 nm spectra in Fig. 1 represents the ground-state transition from $M\mathrm{Au}_{12}^-$ to $M\mathrm{Au}_{12}$, from which we were able to evaluate the ADEs and VDEs (ADEs—adiabatic electron detachment energies), as given in Table I. The ADEs represent the electron affinities of the neutral $M\mathrm{Au}_{12}$ clusters. The extremely high electron affinities for $M\mathrm{Au}_{12}$ (M=V,Nb,Ta) are in accord with the fact that the $M\mathrm{Au}_{12}^-$ anions are highly electronically stable and they are closed-shell systems with 18 valence electrons.

TABLE I. Observed adiabatic (ADE) and vertical (VDE) detachment energies in eV from anion photoelectron spectra of $M\mathrm{Au}_{12}^-$ (M=V,Nb,Ta). The numbers in parentheses represent the experimental uncertainties in the last digit.

	Observed features	VAu_{12}^-	NbAu_{12}^-	TaAu_{12}^-
ADE[a]	X	3.70 (3)	3.77 (3)	3.76 (3)
VDE	X	3.79 (2)	3.88 (2)	3.90 (2)
	A	5.08 (4)	5.14 (4)	5.19 (4)
	B	5.39 (3)	5.48 (3)	5.53 (3)
	C	5.63 (3)	5.71 (3)	5.76 (3)
	D	5.77 (3)	5.82 (3)	5.87 (3)
	E	6.21 (3)	~6.28	~6.25

[a]The ADE of an anion also represents the electron affinity of the corresponding neutral species.

The 193 nm spectrum of VAu_{12}^- [Fig. 1(d)] revealed numerous bands at higher binding energies (labeled as A, B, C, D, and E), which are well separated with the ground-state transition (X). The A band at a VDE of 5.08 eV represents the first excited state of neutral VAu_{12} and the other features correspond to higher excited states. Since the weak features due to contamination were not well resolved, we were confident that the well-resolved higher binding energy bands were due to the main isomer of VAu_{12}^-. Similar higher binding energy features were also observed in the 193 nm spectra of NbAu_{12}^- [Fig. 1(e)] and TaAu_{12}^- [Fig. 1(f)]. In fact, all the observed PES features for the three systems have a one-to-one correspondence to each other and they also have very similar VDEs, as given in Table I. The similarity of the spectral patterns for the three systems is further proof that they were indeed from the $M\mathrm{Au}_{12}^-$ species. As shown below, these spectral patterns are well reproduced from the theoretically simulated PES spectrum for the I_h $\mathrm{Ta@Au}_{12}^-$ cluster.

IV. THEORETICAL RESULTS

One of the most important questions that we want to address here is to confirm the lowest energy structures of the $M\mathrm{Au}_{12}^-$ clusters. While exohedral structures for $M\mathrm{Au}_{12}^-$ are obviously less stable, the endohedral structures can adopt several different geometries, including those with I_h, O_h, and D_{5h} symmetries, as we have shown previously for WAu_{12} and MoAu_{12}.[18] Our previous study indicated that although the I_h structure is preferred for $\mathrm{Mo@Au}_{12}$ and $\mathrm{W@Au}_{12}$, the O_h structure is very close in energy to the global minimum I_h structure. We therefore performed all-electron DFT calculations on the closed-shell $M\mathrm{Au}_{12}^-$ (M=V,Nb,Ta) anions with different endohedral structures to search for the global minima. We found that the icosahedral structures are always favored even without symmetry restrictions during the geometry optimizations. The computed ADF total energies and relative energies from scalar-relativistic and spin-orbit coupling calculations are listed in Table II.

The geometry parameters, total energies, VDEs, and ADEs of the I_h anions and D_{5d} neutrals calculated from the NWCHEM program are listed in Table III. The optimized structures of $\mathrm{Ta@Au}_{12}^-$ with I_h, O_h, and D_{5h} symmetries are shown in Fig. 2, the calculated valence molecular orbital energy levels of $M\mathrm{@Au}_{12}^-$ (M=V,Nb,Ta) are depicted in Fig. 3, and the simulated PES spectrum of $\mathrm{Ta@Au}_{12}^-$ is given in Fig. 4.

V. DISCUSSION

A. Comparison of the PES spectrum of $\mathrm{Ta@Au}_{12}^-$, $\mathrm{W@Au}_{12}^-$, and Au_{13}^-

It is instructive to compare the PES spectra of $M\mathrm{Au}_{12}^-$ (M=V,Nb,Ta) with those of $\mathrm{W@Au}_{12}^-$ and Au_{13}^-, which we have characterized previously.[8,18] In Fig. 5, we compare the 193 nm PES spectra of VAu_{12}^- with those of $\mathrm{W@Au}_{12}^-$ (Ref. 18) and Au_{13}^- (Ref. 8). The similarities and differences between the spectra of VAu_{12}^- and $\mathrm{W@Au}_{12}^-$ are

TABLE II. PW91 total energies and relative energies of $M@Au_{12}^-$ (M=V,Nb,Ta) ions calculated using ADF with all-electron TZ2P basis sets. The scalar-relativistic (SR) and spin-orbit (SO) coupling calculations were both performed with ZORA approximation (see text). The total energies (in eV) are relative to the restricted atomic fragments, and the relative energies (in kJ/mol) are those relative to the respective total energies of the icosahedral structure (I_h).

		E_{tot}(SR)	ΔE(SR)	E_{tot}(SO)	ΔE(SO)
$V@Au_{12}^-$	I_h	−39.8091	0.00	−10 564.3068	0.00
	O_h	−39.5963	20.53	−10 563.9801	31.52
	D_{5h}	−39.4019	39.29	−10 563.8084	48.09
$Nb@Au_{12}^-$	I_h	−42.3900	0.00	−10 575.2088	0.00
	O_h	−42.3427	4.56	−10 575.0822	12.21
	D_{5h}	−42.2422	14.25	−10 574.9830	21.78
$Ta@Au_{12}^-$	I_h	−42.0502	0.00	−11 084.5739	0.00
	O_h	−41.9281	11.78	−11 084.3948	17.28
	D_{5h}	−41.8724	17.16	−11 084.3335	23.19

immediately revealed: except for the very low binding energy band at 2.1 eV for $W@Au_{12}^-$ [Fig. 5(b)], its higher binding energy features show obvious similarity to the spectral features of VAu_{12}^-. VAu_{12}^- and WAu_{12} are valent isoelectronic—both are closed shell with 18 electrons. The low binding energy band in the spectrum of WAu_{12}^- is due to the extra electron that occupies the LUMO of WAu_{12}. The similarity of the higher binding energy part of the two spectra suggests they have similar molecular orbital energy levels, i.e., similar symmetry and geometrical structures. In fact, the V-Au distance (2.761 Å) in $I_h\,V@Au_{12}^-$ and that (2.755 Å) in $I_h\,W@Au_{12}$ are nearly identical. The spectrum of VAu_{12}^- is in fact simpler than that of WAu_{12}^- because VAu_{12}^- is closed shell and only doublet neutral states are allowed upon photodetachment, whereas WAu_{12}^- has a doublet ground state and both singlet and triplet neutral states are produced in the PES spectrum.

The bandwidth of the ground-state transition (X) in the spectra of VAu_{12}^- and WAu_{12}^- reflects the Jahn-Teller distortions in VAu_{12} and WAu_{12}^-, which both possess degenerate electronic states in the I_h symmetry and are subject to Jahn-Teller instability. However, there are major differences in the two systems in terms of the photodetachment transitions: in the former the Jahn-Teller effect is in the final neutral states, whereas in the latter it is in the initial anionic state. In WAu_{12}^-, the detachment transition takes place from the ground state of the Jahn–Teller-distorted $D_{5d}\,WAu_{12}^-$ and the ground-state PES spectral transition reflects the geometrical changes between the $D_{5d}\,WAu_{12}^-$ and the $I_h\,WAu_{12}$. Since the geometrical structural changes are very small, a very sharp ground-state transition was observed in the 532 nm spectrum of WAu_{12}^- previously.[18] On the other hand, for VAu_{12}^- the detachment transition happens from the $I_h\,VAu_{12}^-$. The neutral final VAu_{12} state is not Jahn-Teller stable under I_h symmetry and would distort to D_{5d}, splitting the final states. The electronic state splitting is seen clearly from the simulated spectrum (Fig. 4), which agrees well with the relatively broad spectral width of the X band in the PES spectra of $TaAu_{12}^-$, as well as in those of VAu_{12}^- and $NbAu_{12}^-$.

On the other hand, the spectrum of Au_{13}^- [Fig. 5(c)] is much more complicated with many more features, which display no resemblance to either the spectrum of VAu_{12}^- or WAu_{12}^-. Ion mobility experiment[6] has ruled out either a planar or an I_h structure for Au_{13}^-, which is likely to have a low symmetry 3D structure, commensurate with its complicated PES spectrum.

TABLE III. Optimized M-Au bond lengths, B3LYP total energies for the $I_h\,M@Au_{12}^-$ anions and the D_{5d} neutrals, and the adiabatic (ADE) and vertical (VDE) electron detachment energies for the anions calculated by using NWCHEM. The bond lengths are in Å. The total energies are in hartree and ADEs and VDEs are in eV. All the anions are optimized with I_h symmetry and the neutral clusters with D_{5d} symmetry.

	M-Au	E_{tot}	ADE	VDE
$V@Au_{12}$	2.736×2, 2.765×10	−1703.196 44	⋯	⋯
$Nb@Au_{12}$	2.786×2, 2.804×10	−1688.569 20	⋯	⋯
$Ta@Au_{12}$	2.784×2, 2.806×10	−1688.614 53	⋯	⋯
$V@Au_{12}^-$	2.761×12	−1703.323 46	3.46	3.47
$Nb@Au_{12}^-$	2.804×12	−1688.702 69	3.63	3.65
$Ta@Au_{12}^-$	2.805×12	−1688.748 64	3.65	3.66

B. Electronic structure and energy-level diagram of the icosahedral $M@Au_{12}^-$ clusters

Our theoretical calculations indicate that all the MAu_{12}^- (M=V,Nb,Ta) anions prefer the icosahedral structure, with the energies of the O_h and D_{5h} structures being higher (Table II). With the increase of the central atom size, the energy difference between the O_h and the I_h structures tends to diminish, consistent with the enhanced M-Au interaction in the O_h structure. However, this trend is clearly offset by the increased relativistic and aurophilic effects,

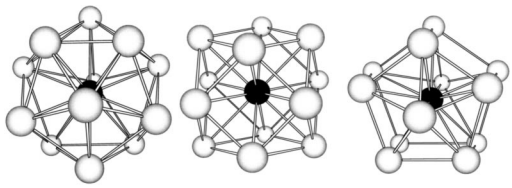

FIG. 2. Optimized geometry structures of $Ta@Au_{12}^-$ with different point-group symmetries: (a) I_h, (b) O_h, (c) D_{5h}.

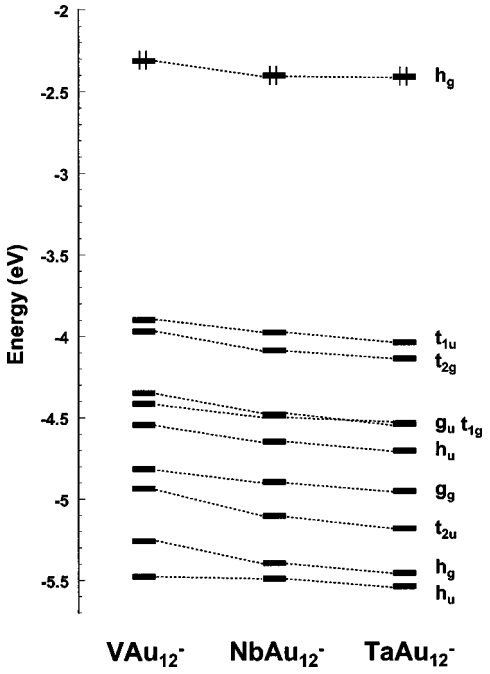

FIG. 3. Calculated energy-level diagrams of valence molecular orbitals of $M@Au_{12}^-$ (M=V,Nb,Ta). The h_g levels shown with electron occupations correspond to the fivefold degenerate HOMOs.

which favor the I_h structure with its favorable Au-Au interactions. Interestingly, the spin-orbit coupling effects tend to stabilize the I_h structure relative to the O_h and D_{5h} structures. The calculated ADEs and VDEs agree well with the experiment, in particular for those of I_h Nb@Au_{12}^- and Ta@Au_{12}^-. The calculated values for I_h V@Au_{12}^- are slightly lower than the experiment.

The calculated molecular orbital energy-level diagrams for the three I_h $M@Au_{12}^-$ species (Fig. 3) are nearly identical, which underlies the similarities of their PES spectra in Fig. 1. The molecular orbital energy-level diagrams are in qualitative agreement with the PES spectra. The ground-state peak (X) in the PES spectra is due to electron detachment from the HOMO (h_g), whereas the A band in the PES spectra is due to detachment from HOMO-1 (t_{1u}). The large

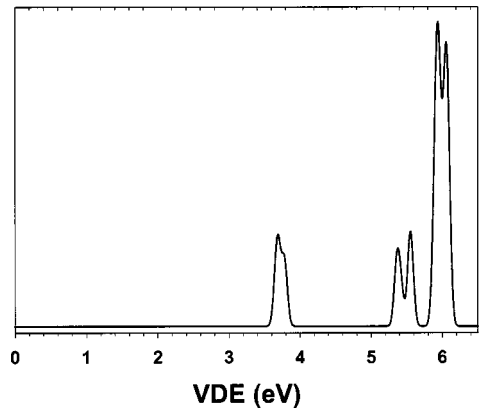

FIG. 4. Simulated electron detachment spectrum for Ta@Au_{12}^-. The spectrum was constructed by fitting the distribution of the calculated vertical detachment energies with unit-area Gaussian functions of 0.04 eV full width at half maximum.

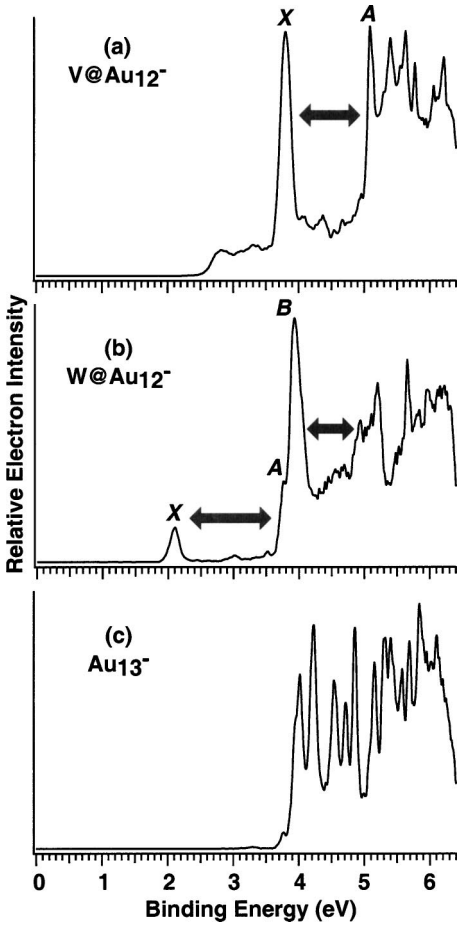

FIG. 5. Comparison of the photoelectron spectra of (a) VAu_{12}^-, (b) $W@Au_{12}^-$, and (c) Au_{13}^- at 193 nm. The arrows denote the observed energy gaps. The spectra of $W@Au_{12}^-$ and Au_{13}^- are taken from Refs. 18 and 8, respectively.

h_g-t_{1u} energy separation is consistent with the observed large X-A separation. The closely-lying orbitals below HOMO-1 are also in agreement with the observed spectral patterns at the higher binding energy side. We further calculated state-specific VDEs to simulate the PES spectra of Ta@Au_{12}^-, as shown in Fig. 4. Clearly, the overall pattern of the simulated spectrum compares well with the experimental spectrum. The high electron affinity, the prominent threshold band X, and the large X-A energy gap were all reproduced by the simulation. The excellent agreement between the molecular orbital energy levels, as well as the simulated spectrum, and the experimental spectra lend considerable credence to the global minimum I_h structures of the MAu_{12}^- clusters and confirmed the correct identification of the main spectral features of MAu_{12}^- in Fig. 1. Since the cluster temperatures were expected to be at room temperature, the O_h isomer may also have a small contribution to the weak features, in particular, in the spectra of $NbAu_{12}^-$ and $TaAu_{12}^-$.

VI. CONCLUDING REMARKS

Despite the high stabilities of the I_h $M@Au_2^-$ clusters, the 12 Au atoms forming the icosahedral cage appear to be rather fluxional, as evidenced by the closely-lying O_h and D_{5h} structures. The O_h isomer involves a slight rearrange-

ment of the 12 Au atoms on the cage, whereas the D_{5h} structure involves a rotation of a hemisphere of the I_h Au_{12} cage against each other. The corresponding h_u vibrational mode is predicted to have a very low frequency around 30 cm^{-1}.[17] We calculated the frequencies for the corresponding vibrational modes in $M@Au_{12}^-(M=V,Nb,Ta)$ to be 37, 27, and 27 cm^{-1}, respectively. It is interesting to note that only for VAu_{12}^- the I_h cage structure is significantly more stable than either the O_h or the D_{5h} structure.

Heretofore we have confirmed and characterized two of the three $M@Au_{12}(M=Ta^-,W,Re^+)$ cage clusters originally predicted by Pyykko and Runeberg.[14] Furthermore, we have extended this family of clusters to include $4d$ and $3d$ heteroatoms. The confirmation of their existence as highly stable gaseous molecules suggests that they may exist in the bulk form or on surfaces. The charged cage clusters, either $M@Au_{12}^-$ or $M@Au_{12}^+$, may be more promising for potential bulk syntheses because the coulomb repulsion between two charged clusters and the necessity of counterions are both advantageous in keeping the cages from fusion in the bulk.

ACKNOWLEDGMENTS

This work was supported by the National Science Foundation (CHE-0349426) and performed at the W. R. Wiley Environmental Molecular Sciences Laboratory (EMSL), a national scientific user facility sponsored by DOE's Office of Biological and Environmental Research and located at Pacific Northwest National Laboratory, operated for DOE by Battelle. All calculations were performed with supercomputers at the EMSL Molecular Science Computing Facility.

[1] M. Haruta, Catal. Today **36**, 153 (1997), and references therein.
[2] For a recent highlight on nanogold, see P. Schwerdtfeger, Angew. Chem., Int. Ed. **42**, 1892 (2003).
[3] P. Pyykkö, Chem. Rev. (Washington, D.C.) **88**, 563 (1988).
[4] H. Schmidbaur, Gold Bull. (London) **33**, 3 (2000).
[5] H. Hakkinen, M. Moseler, and U. Landman, Phys. Rev. Lett. **89**, 033401 (2002).
[6] F. Furche, R. Ahlrichs, P. Weis, C. Jacob, T. Bierweiler, and M. Kappes, J. Chem. Phys. **117**, 6982 (2002).
[7] H. M. Lee, M. Ge, B. R. Sahu, P. Tarakeshwar, and K. S. Kim, J. Phys. Chem. B **107**, 9994 (2003).
[8] H. Hakkinen, B. Yoon, U. Landman, X. Li, H. J. Zhai, and L. S. Wang, J. Phys. Chem. A **107**, 6168 (2003).
[9] L. Xiao and L. Wang, Chem. Phys. Lett. **392**, 452 (2004).
[10] J. Li, X. Li, H. J. Zhai, and L. S. Wang, Science **299**, 864 (2003).
[11] H. F. Zhang, M. Stender, R. Zhang, C. Wang, J. Li, and L. S. Wang, J. Phys. Chem. B **108**, 12259 (2004).
[12] M. P. Johansson, D. Sundholm, and J. Vaara, Angew. Chem., Int. Ed. **43**, 2678 (2004).
[13] X. Gu, M. Ji, S. H. Wei, and X. G. Gong, Phys. Rev. B (in press).
[14] P. Pyykkö and N. Runeberg, Angew. Chem., Int. Ed. **41**, 2174 (2002).
[15] D. M. P. Mingos, J. Chem. Soc. Dalton Trans. **1976**, 1163.
[16] C. E. Briant, B. R. C. Theobald, J. W. White, L. K. Bell, D. M. P. Mingos, and A. J. Welch, J. Chem. Soc., Chem. Commun. **1981**, 201.
[17] J. Autschbach, B. A. Hess, M. P. Johansson, J. Neugebauer, M. Patzschke, P. Pyykkö, M. Reiher, and D. Sundholm, Phys. Chem. Chem. Phys. **6**, 11 (2004).
[18] X. Li, B. Kiran, J. Li, H. J. Zhai, and L. S. Wang, Angew. Chem., Int. Ed. **41**, 4786 (2002).
[19] L. S. Wang, H. S. Cheng, and J. Fan, J. Chem. Phys. **102**, 9480 (1995).
[20] L. S. Wang and H. Wu, in *Advances in Metal and Semiconductor Clusters. IV. Cluster Materials*, edited by M. A. Duncan (JAI, Greenwich, CT, 1998), pp. 299–343.
[21] ADF 2003.01, SCM, Theoretical Chemistry, Vrije Universiteit, Amsterdam, The Netherlands (http://www.scm.com).
[22] G. te Velde, F. M. Bickelhaupt, S. J. A. van Gisbergen, C. Fonseca Guerra, E. J. Baerends, J. G. Snijders, and T. Ziegler, J. Comput. Chem. **22**, 931 (2001).
[23] C. Fonseca Guerra, J. G. Snijders, G. te Velde, and E. J. Baerends, Theor. Chem. Acc. **99**, 391 (1998).
[24] T. P. Straatsma, E. Apra, T. L. Windus *et al.*, NWCHEM, A Computational Chemistry Package for Parallel Computers, Version 4.5, 2003, Pacific Northwest National Laboratory, Richland, Washington 99352-0999, USA.
[25] J. P. Perdew and Y. Wang, Phys. Rev. B **45**, 13244 (1992).
[26] J. P. Perdew, J. A. Chevary, S. H. Vosko, K. A. Jackson, M. R. Pederson, D. J. Singh, and C. Foilhais, Phys. Rev. B **46**, 6671 (1992).
[27] E. van Lenthe and E. J. Baerends, J. Comput. Chem. **24**, 1142 (2003).
[28] E. van Lenthe, E. J. Baerends, and J. G. Snijders, J. Chem. Phys. **99**, 4597 (1993).
[29] A. D. Becke, J. Chem. Phys. **98**, 1372, 5648 (1993).
[30] C. Lee, G. Yang, and R. G. Parr, Phys. Rev. B **37**, 785 (1988).
[31] P. J. Stephens, F. J. Devlin, C. S. Ashvar, C. F. Chabalowski, and M. J. Frisch, Faraday Discuss. **99**, 103 (1994).
[32] P. J. Stephens, F. J. Devlin, C. F. Chabalowski, and M. J. Frisch, J. Phys. Chem. **98**, 11 623 (1994).
[33] D. Andrae, U. Haeussermann, M. Dolg, H. Stoll, and H. Preuss, Theor. Chim. Acta **77**, 123 (1990).
[34] M. Dolg, U. Wedig, H. Stoll, and H. Preuss, J. Chem. Phys. **86**, 866 (1987).
[35] J. M. L. Martin and A. Sundermann, J. Chem. Phys. **114**, 3408 (2001).
[36] M. E. Casida, C. Jamorski, K. C. Casida, and D. R. Salahub, J. Chem. Phys. **108**, 4439 (1998).
[37] D. J. Tozer and N. C. Handy, J. Chem. Phys. **109**, 10180 (1998).
[38] S. Hirata, Z. G. Zhan, E. Apra, T. L. Windus, and D. A. Dixon, J. Phys. Chem. A **107**, 10154 (2003).
[39] J. Li, J. Cluster Sci. **13**, 137 (2002).
[40] M. E. Casida and D. R. Salahub, J. Chem. Phys. **113**, 8918 (2000).
[41] C. G. Zhan, J. A. Nichols, and D. A. Dixon, J. Phys. Chem. A **107**, 4184 (2003).